Mechanical Behavior of Slender Concrete-Filled Fiber Reinforced Polymer Columns

Sokhwan Choi[1], Myung Lee[2], and Sung-Woo Lee[1]

[1] Dept. of Civil and Environmental Engineering, Kookmin Univ., 861-1 Chongnung-dong, Songbuk-ku, Seoul, Korea
[2] Kookmin Composite Infrastructure, Inc., 770-17, Yeoksam-Dong, Gangnam-Gu, Seoul, Korea

Abstract

The mechanical behavior of concrete-filled glass fiber reinforced polymer columns is affected by various factors including concrete strength, stiffness of tube, end confinement effect, and slenderness ratio of members. In this research the behavior of slender columns was examined both experimentally and analytically. Experimental works include 1) compression test with 30cm long glass fiber composite columns under different end confinement conditions, 2) uni-axial compression test for 7 slender columns, which have various slenderness ratios. Short-length stocky columns gave high strength and ductility revealing high confinement action of FRP tubes. The strength increment and strain change were examined under different end confinement conditions. With slender columns, failure strengths, confinement effects, and stress-strains relations were examined. Through analytical work, effective length was computed and it was compared with the amount of reduction in column strength, which is required to predict design strength with slender specimens. This study shows the feasibility of slender concrete-filled glass fiber reinforced polymer composite columns.

1. Introduction

Researchers have introduced concrete-filled glass fiber reinforced polymer (GFRP) composite tubes (CFFT) to overcome the corrosion and deterioration of steel tubes under harsh environmental conditions.[1-5] Benefits in using CFFTs may include low maintenance costs, high earthquake resistance, and long expected endurance period. Even though the application of fiber reinforced polymer as part of the construction materials is quite promising, it is difficult to generalize the structural parameters for members using GFRP shells. It is mainly because the fabrication skills that people apply are not directly comparable each other, and furthermore, the filled-in concrete shows complex compressive behavior under multi-axially confined stress condition. In the current study, the mechanical behavior of slender concrete-filled GFRP columns was studied. With relatively short specimens, which have the length of 30cm, the confinement effect on the stress-strain relation of concrete was

studied first. In this test, three different shear confinement conditions were adopted and test results were compared each other. Next, slender specimens with various lengths were tested and the reduction in strength was analyzed according to the slenderness ratios of members through analytical methods.

2. Specimens prepared for each experimental work

Three different categories of specimens-stocky CFFT specimens, various slender columns, and plain concrete cylinders-were prepared as follows. Detailed descriptions about those specimens are as follows, and more information is given in Table 1.

1) 9 CFFT specimens that have the length of 30cm were fabricated. These specimens are used to obtain the stress-strain relation of concrete under confinement action provided by the GFRP tube. Since the mechanical response is dependent on the shear confinement at end surfaces of a specimen,[6] three different end conditions were examined as shown later. The inner diameter of

* Corresponding author
Tel.: +82-2-910-4648   Fax.: +82-2-910-4939
E-mail address: shchoi@kookmin.ac.kr

tube is 165mm. The thickness or fiber alignment of GFRP tube was not a parameter for the current research, and it is fixed as 6.5mm. Fig. 1 represents the test set-up.

2) 8 CFFT slenderness test specimens of which lengths were 590mm, 1260mm, 1920mm, and 2590mm were fabricated and tested. Fig. 2 depicts the slenderness test specimen.

3) Several plain concrete specimens were prepared and tested to measure the uniaxial strength of concrete.

The shear confinement that exists between the loading platens and a specimen introduces the barrel effect, and therefore, in order to obtain uniaxial material behavior it should be removed. Three different end conditions are denoted as GR, GT, and NG. End condition, GR, in Table 1 means the test case where each ends of 30cm GFRP tube was cut off by 1cm, and only bare concrete was contact to loading platens. In GT case, tubes were cut off at both sides by 1cm similar to GR, but Teflon sheets were also used between the loading platen and specimen in order to further remove the shear confinement.
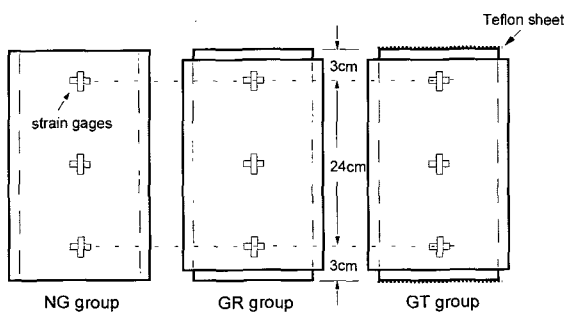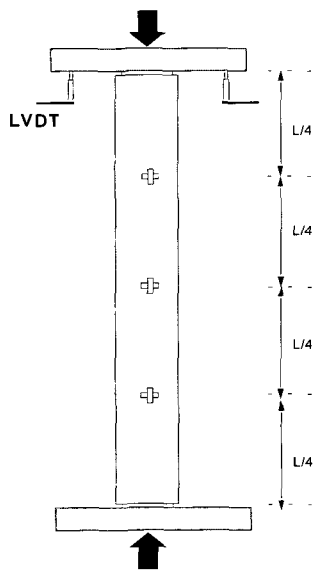

Fig. 1 30cm CFFT specimens

Fig. 2 Testing setup for slender columns

In GR specimens, relatively weak end zone would allow lateral expansion and diminish shear confinement. GT specimens were introduced to find if shear confinement can be further removed by Teflon sheets, and see if the results are comparable with those of GR test case. NG is the case that core concrete and tubes were ground at both ends, and lubricant was not applied either. And, therefore, shear confinement will exist at both ends and applied loads will be transferred directly to both core concrete and tube. Mix design for the core concrete is given in Table 2.

Current GFRP tubes were designed to resist against both compression and bending. The composite shells provide plies in both axial and transverse directions, i.e., both longitudinal and circumferential directions. In fabricating the GFRP tubes, E-glass fibers were placed outside a mold (5 plies of 900 gf/m^2) with hand lay-up method, and on top of it, 2 additional plies of fibers were filament wound before the resin (vinyl ester) were hardened.

3. 30cm CFFT specimen test and results

5,000kN servo hydraulic material testing machine was used for this experiment. The loading rate was kept constant as a strain rate of 0.001/min. It means that faster deformation was applied for longer specimens. All concrete specimens will show large deformation at the initial part of the loading due to fixture connection, interface between loading platen and specimen, and soft casting boundary of concrete specimens. This phenomenon is not directly related to the behavior of specimen and was removed by pre-loading.

Table 1 Specimens prepared for the experiment

Experiment category	End condition	Length (mm)	Number of specimens	Fixation of fixture
30cm CFFT specimen	GR, GT, NG	300	3 for each end condition	Rotating top and fixed bottom
Slender CFFT specimen	Grinding and gypsum capping	590, 1260, 1920, 2590	2 for each length	Fixed at top and bottom
Plain concrete cylinder	Grinding	200	Several	Rotating top and fixed bottom

Table 2 Mix proportion of filled-in concrete

Max. aggregate size(mm)	Slump (cm)	Air contents (%)	W/B (%)	Weight of ingredients (kgf/m³)					
				W	C	S	G	Fly ash	AE
25	12.0	4.5	44.8	176	363	744	940	50	4.13

(a) Dring testing   (b) A failure

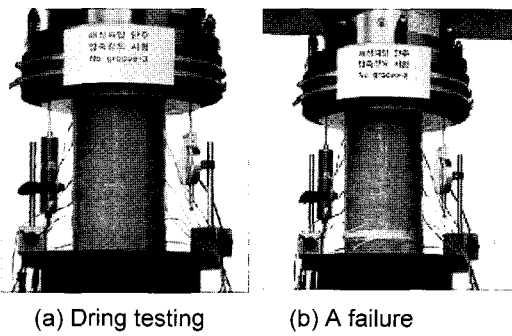**Fig. 3** Setup for a NG specimen

(a) Duing testing   (b) A failure
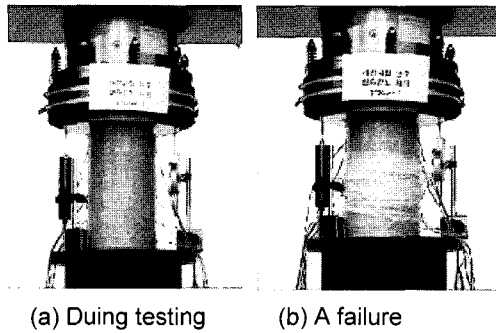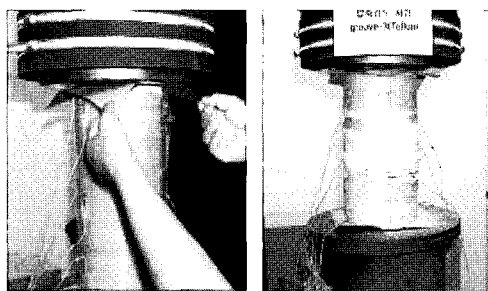
Fig. 4 Setup for a GR specimen

(a) insertion of Teflon sheets   (b) at failure

Fig. 5 Setup for a GT specimen

Table 3 30cm CFFT specimen test results

I.D.	Age (day)	P_u [MN]	f_u [MPa]	ε_u	$\dfrac{f_u}{f_{cu}}$
NG_1	71	2.106	98.6	0.017	3.50
NG_2	71	2.227	104.2	0.014	3.70
NG_3	71	2.165	101.3	0.014	3.59
GR_1	72	2.177	101.9	0.047	3.61
GR_2	72	2.165	101.3	0.049	3.59
GR_3	72	2.146	100.4	0.052	3.56
GT_2	72	2.029	94.9	0.044	3.37
GT_3	72	2.063	96.5	0.042	3.42

The magnitude of preloading was 77kN for plain cylinder specimens, and 210kN for 30cm CFFT specimens, which were turned out to be 10% and 34% of the specimen strength, respectively.

The average strength of plain concrete cylinder, f_u, at the age of 71 days was 28.6MPa (28.2MPa, 29.8MPa, 27.8MPa respectively). The axial deformation was measured from LVDT readings attached between top and bottom platens as in Figs. 3 ~ 5, and detailed results are given in Table 3. Two LVDTs were attached at both side of the specimen and readings were averaged to get deformation value at the core center of the specimen removing the effect of platen rotation. The strain values in Fig. 6 were obtained using the deformation measurement obtained form LVDT read-outs.

As is known from similar researches, the failure strength of concrete confined with FRP tube shows much higher strength than plain concrete. The strength of 3.4 ~ 3.6 times higher than plain concrete cylinder was obtained in the experiment too, and the strength values will depend on the magnitude of confinement. As shown in the figure, the ultimate strength of the 30cm CFFT specimens was not a function of end conditions. This is because the final failure is occurred by the tensile fracture of tube, and therefore, the maximum strength of the specimen is determined by the circumferential strength of GFRP tubes, which is identical for all testing specimens. As explained before, both ends of GFRP tubes were cut off by 1cm for GR and GT cases, and the strains at failure differ by shear confinement since no axial force is applied directly to the tube for GR and GT cases, which is contrary to NG case. For NG specimens, force is directly loaded on the tubes and high strains were obtained as shown in Figs. 1, 3.

On the other hand, force is not transferred to the tubes near ends since mechanical and chemical bond between concrete and GFRP tube is weak and debonding is occurred in this area. Strains measured at the middle surface show that after confined pressure is applied to the tubes some axial stress is transferred to the tubes from concrete, and generate axial strain values.

Figs. 9, 10 show the axial and circumferential strains at failure. Even though the final fracture ends at the tensile failure of tubes, fracture does not occur through the whole specimen height simultaneously, and the circumferential strain values are not exactly the same as is shown in Fig. 9.

Based on aforementioned various observations, it can be concluded that Teflon sheets inserted for GT group did not play any significant role in overall behavior comparing GR group. And GR method, which is simpler, was selected for the end conditions of slenderness test specimens.
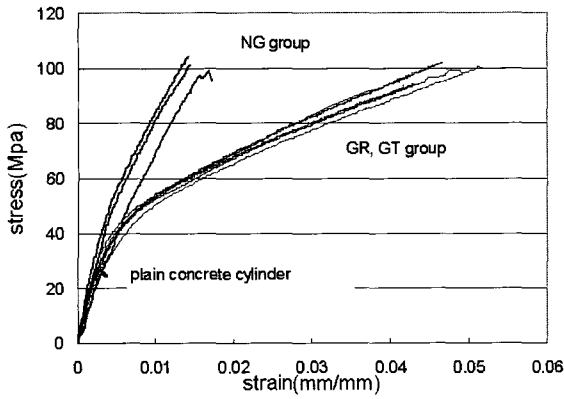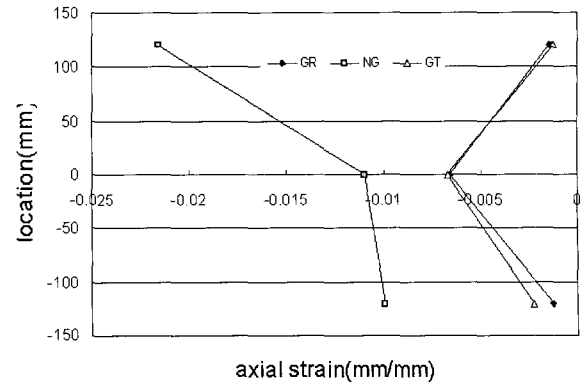
Fig. 6 Stress-strain relation of 30cm CFFT tubes

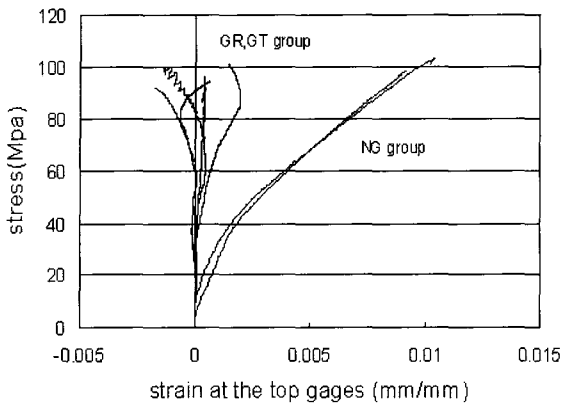**Fig. 9** Axial strains at each gage location at final stage
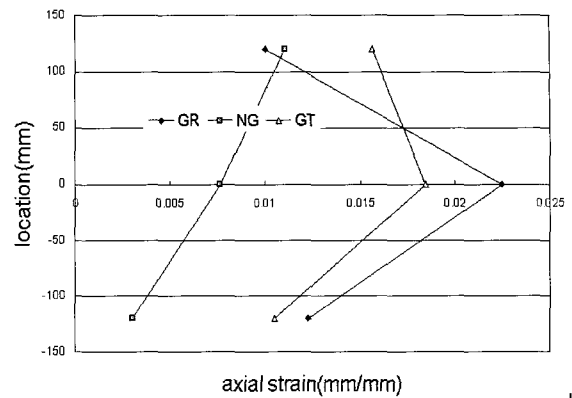

Fig. 7 Axial strains at the top gages of 30cm CFFT

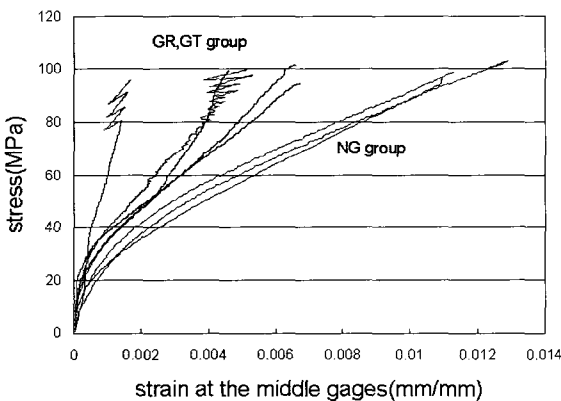**Fig. 10** Circumferential strains at each gage location at final stage

Fig. 8 Axial strains at the middle gages of 30cm CFFT

Table 4 Experimental results from slenderness test

I.D	Length (mm)	Loading rate (mm/min)	Age (day)	P_u (MN)	f_u (MPa)	ε_u
590_1	590	0.59	63	2.095	98.1	0.0412
590_2	590	0.59	63	2.041	95.5	0.0442
1260_1	1260	1.26	64	1.843	86.3	0.0252
1260_2	1260	1.26	64	1.996	93.5	0.0278
1920_2*	1920	1.92	64	1.505	70.4	0.0178
2590_1	2590	2.59	65	1.118	52.3	0.0115
2590_2	2590	2.59	65	1.126	52.7	0.0094

* The test for 1920-1 specimen was not completed properly and discarded from analysis.

4. Slenderness test and results

A universal testing machine which has the capacity of 5,000kN was used for this experiment. Loading platens at both ends were not rotatable, and it was confirmed by measuring rotation with auxiliary gages during testing.

Experimental data obtained from this slenderness test is shown in Table 4. Specimen I.D. is named based on the member length. Various lengths of specimens were tested,

and maximum strength and strains were measured at various gage locations.

Photos obtained during testing for each member were given in Fig 11. It should be noted that both ends of columns were simply gypsum capped to fill the gap between the member and loading platens and assure more uniform stress distribution. In this setup, since no tensile force can be transferred, end moment is generated by the eccentricity of axial load only.
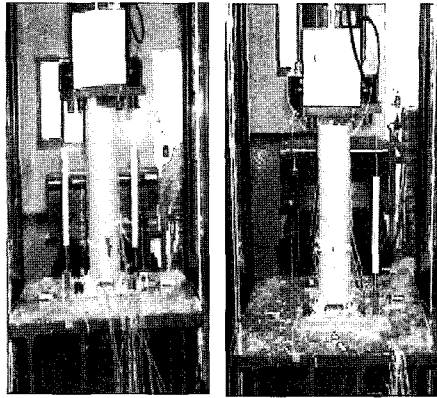
(a) 590-1 (testing)   (b) 590-2 (at failure)
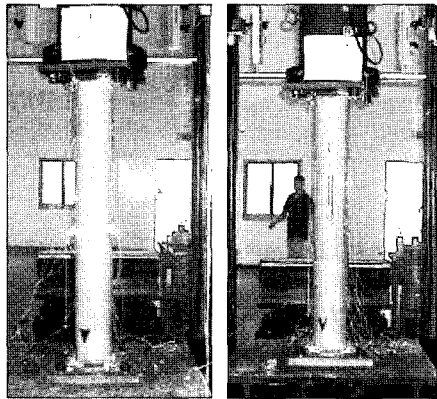
(c) 1260-1 (at failure) (d) 1260-2 (testing)

(e) 1920-2(at failure) (f)2590-1 (at failure) (g)2590-2 (testing)

Fig. 11 Photos taken at the experiment site

It means that both ends were not fixed, and effective length of a column is not half of the member length. This phenomenon can be confirmed in the photos again.

Fig. 12 is the load-deformation relations of slender specimens. Strain values were obtained by measuring the movement of top loading platen against fixed bottom platen.
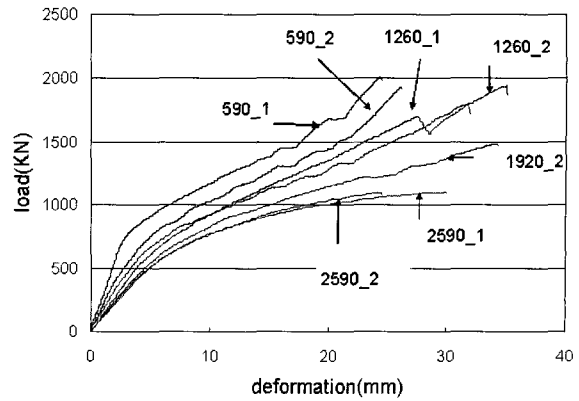

Fig. 12 Load-deformation relations of slender specimens

Fig. 13 Deflected shape of a column under both axial and flexural loading

5. Analysis for slender CFFT columns

As mentioned before, the end condition of the test specimen is not fixed, and, therefore the coefficient of effective length k is not 0.5 since the end moment is not fully transferred to the loading fixture during testing. Effective length will be computed by introducing a analytical model and comparing with experimental read-outs. The deflected shape of the column subjected to axial load P and end moment M_a, as is shown in Fig. 13, can be represented by Eq. (1).[7]

$$f(x) = \frac{M_a}{P} \cdot \left[1 - \tan\left(\frac{k_0 L}{2} \right) \cdot \sin(k_0 x) - \cos(k_0 x) \right] \qquad (1)$$

$$\frac{d^2 f(x)}{dx^2} = \frac{M_a}{P} \cdot k_0^2 \cdot \left[\tan\left(\frac{k_0 L}{2} \right) \cdot \sin(k_0 x) + \cos(k_0 x) \right] \qquad (2)$$

Where, $f(x)$ represents the deflected shape of the column, and $k_0 = \sqrt{\frac{P}{EI}}$ L is the member length. The axial force P is given during testing, and end moment M_a is unknown at this stage.

The following condition applies to the inflection point (i.p.), where the moment and curvature are zeros.

$$\frac{d^2 f(x)}{dx^2} = 0 \tag{3}$$

It gives

$$x = -a \tan\left(\frac{1}{\tan\left(\sqrt{\frac{P}{EI}} \cdot \frac{L}{2}\right)}\right) \cdot \sqrt{\frac{EI}{P}} \tag{4}$$

The total strains at a point, $\varepsilon_t(x)$ is given as follows.

$$\varepsilon_t(x) = \frac{-\dfrac{d^2 f(x)}{dx^2}}{\left[1 + \left(\dfrac{df(x)}{dx}\right)^2\right]^{3/2}} \cdot D \tag{5}$$

The measured total strain due to moment at the middle of a specimen can be compared with this analytical value, and end moment can be obtained. Total strains can not be obtained directly from gages since the bending plane is not known beforehand. Strain gages were attached at the surface of specimen at every 90°, and maximum strain is computed using multi regression analysis based on least square method. After deformation plane is found, the maximum and minimum strains can be calculated.

Multi regression analysis, as is shown in Fig. 14, tells that the regression plane Y to be obtained has a form of $Y = \alpha + \beta_1 X_1 + \beta_2 X_2 + \varepsilon$, where X_1, X_2 are the coordinates for the gage locations, $\overline{X_1}, \overline{X_2}$ are the average of X_1, X_2, respectively. And, $\overline{Y}$ is the average of strain values Y. Other variables are $x_1 = X_1 - \overline{X_1}$, $x_2 = X_2 - \overline{X_2}$, $\alpha = \overline{Y} - \beta_1 \overline{X_1} - \beta_2 \overline{X_2}$,

$$\beta_1 = \frac{\sum x_1 Y\left(\sum x_2^2\right) - \sum x_2 Y\left(\sum x_1 x_2\right)}{\sum x_1^2\left(\sum x_2^2\right) - \left(\sum x_1 x_2\right)^2} \quad \beta_2 = \frac{\sum x_2 Y\left(\sum x_1^2\right) - \sum x_1 Y\left(\sum x_1 x_2\right)}{\sum x_1^2\left(\sum x_2^2\right) - \left(\sum x_1 x_2\right)^2}$$

and ε is the error. Measured data through strain gages are compared with strain values obtained from this analysis and tabulated in Table 5. The maximum and minimum strains at the middle of the column are tabulated in Table 6.

Stiffness EI of the column for the computation of effective slenderness ratio is obtained from a four point bending test using a specimen with a span length of 2,640mm, and it was found that $EI = 294,000 MN \cdot mm^2$ near the failure where it gives the lower bound value for slenderness. Details of this experiment is given in a reference.[8] Radius of gyration r can be computed as follows.[5]
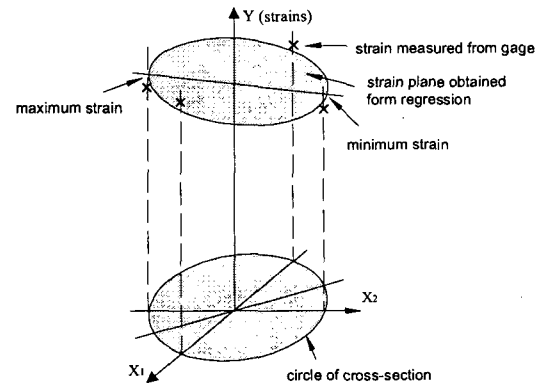

Fig. 14 Multi regression analysis

Table 5 Measured strain data at the middle of the column

I.D	Failure load(kN)	Gage (E)			Gage (W)		
I.D	failure load (kN)	Measured	Regression	Measured/ regression (%)	Measured	Regression	Measured/ regression (%)
2590_1	1.118	-0.0095	-0.0089	106.7	-0.0045	-0.0039	115.4
2590_2	1.126	-0.01208	-0.01152	104.9	-0.0019	-0.00134	141.8
1920_2	1.505	-0.00846	-0.00861	98.3	-0.01021	-0.01036	98.6
1260_1	1.843	-0.00916	-0.00849	107.9	-0.01323	-0.01256	105.3
1260_2	1.996	-0.01542	-0.01569	98.3	-0.01321	-0.01349	97.9
590_1	2.095	-0.00925	-0.00884	104.6	-0.01566	-0.01525	102.7
590_2	2.041	-0.01256	-0.01314	95.6	-0.00765	-0.00823	93

I.D	Failure load(kN)	Gage (S)			Gage (N)		
I.D	Failure load(kN)	Measured	Regression	Measured/ regression (%)	Measured	Regression	Measured/ regression (%)
2590_1	1.118	-0.01693	-0.01693	96.5	0.00473	0.00413	114.5
2590_2	1.126	-0.01045	-0.01101	94.9	-0.00128	-0.00184	69.6
1920_2	1.505	-0.00167	-0.00153	109.2	-0.01759	-0.01744	100.9
1260_1	1.843	-0.0115	-0.01217	94.5	-0.00821	-0.00888	92.5
1260_2	1.996	-0.0141	-0.01382	102	-0.01563	-0.01536	101.8
590_1	2.095	-0.01165	-0.01206	96.6	-0.01162	-0.01203	96.6
590_2	2.041	-0.01279	-0.01086	117.8	-0.00973	-0.01051	92.6

Table 6 Maximum and minimum strain of tested columns

I.D	Failure load (kN)	Max.		Min.		(max+min) /2	max-min
		Angle*(°)	ε	Angle*(°)	ε	ε	ε
2590_1	1.118	103.1	0.00442	283.1	-0.0172	-0.0064	0.02162
2590_2	1.126	138.0	0.00042	318	-0.0133	-0.00643	0.01372
1920_2	1.505	276.3	-0.00148	96.3	-0.0175	-0.00949	0.01602
1260_1	1.843	38.9	-0.0079	218.9	-0.0132	-0.01053	0.0053
1260_2	1.996	214.7	-0.01325	34.7	-0.0159	-0.01459	0.00265
590_1	2.095	3.1	-0.00884	183.1	-0.0153	-0.01205	0.00646
590_2	2.041	148.1	-0.00779	328.1	-0.0136	-0.01069	0.00581

* Angle is measured from the gage E(East) to N(North) direction

Table 7 Coefficient of effective slenderness length

| I.D.	P_u [MN]	k	$\dfrac{kl}{r}$	$\dfrac{P_u}{P_0}$
2590_1	1.12	0.62	36.1	0.518
2590_2	1.13	0.62	36.1	0.522
1920_2	1.51	0.72	31.1	0.698
1260_1	1.84	0.997	28.2	0.851
1260_2	2.00	0.956	27.1	0.925

$$r = \sqrt{\frac{I_g}{A_g}} = \frac{D_{eq}}{4} \quad (6), \qquad D_{eq} = D + 2t\frac{E_f}{E_c} \quad (7)$$

Where, I_g and A_g are gross moment of inertia and area of the section, respectively. D_{eq} is the equivalent diameter of the section based on the transformed areas of the concrete and GRFP tube. D is the inner diameter of tube, t is the thickness of the tube. E_c and E_f are moduli of elasticity of concrete and GRFP tube in compression, respectively. E_c is given as follows.

$$E_c = 4,700\sqrt{f_{ck}} \quad [\text{MPa}] \tag{8}$$

where, the strength of plain concrete cylinder was used for f_{ck}. The coefficient of effective length, k, is calculated by matching maximum value of measured strain (Table 6) is equal to the strains calculated analytically (Eq. 5) for each specimen through trial and error programming. Calculated coefficients of effective slenderness length according to the specimen lengths are tabulated as below, and also in Fig. 15. P_0 is $2.163MN$, which is obtained by averaging the strengths of all three GR specimens.

Five percent reduction in axial strength is the usual criterion to decide whether slenderness effect should be accounted for design.[10] Slenderness ratio, $\dfrac{kl}{r}$, of about 27 corresponds to 5% strength reduction in the current study. Samaan et al.[9] and Mirmiran[5] obtained less than 20 depending on modular ratio of GFRP tube and concrete in similar researches. Authors believe that less slenderness ratio was obtained with the same ultimate strength because they assumed $k = 0.5$, which is the case of fixed-end condition, even though full transfer of end moment was not guaranteed in their setup.
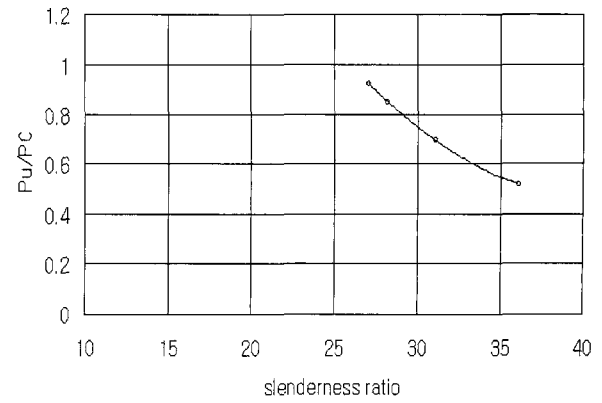
Fig. 15 Effect of slenderness ratio on the strength reduction

6. Summary and conclusions

The slenderness effect of concrete-filled glass fiber reinforced polymer tubes was examined in this study. The feasibility of concrete-filled composite compression members as an alternative to conventional steel or concrete compression members in corrosive environments is shown, and this work provides an experimental database for FRP composite tubes that are externally reinforced by multidirectional fiber composites.

The coefficient of effective length should be computed properly according to the end condition adopted for the experiment. Following conclusions can be drawn;

1) The axial strength of the concrete-filled GFRP tubes increases by a large amount due to the confinement effect given to concrete by the FRP cell. It confirms previous researches.
2) The strengths at failure are dependent on the tensile strength of GFRP tubes, and end loading conditions do not affect on the final strength of specimen.
3) 5% strength reduction occurs with much slenderer CFFTs comparing with reinforced concrete columns.

Acknowledgments

References

1. Mirmiran, A., Samaan, M., and Shahawy, M., "Model of concrete confined by fiber composites," *ASCE Structural Engineering*, Vol.124, No.9, 1998, pp.1025~1031.

2. Mirmiran, A., Shahawy, M., and Samaan, M., "Effect of column parameters on FRP confined concrete," *J. Struct. Engrg., ASCE*, Vol.124, No.9, 1998, pp.1025~1031.

3. Mirmiran, A., Shahawy, M., and Samaan, M., "Behavior of Concrete Columns by Fiber Composite," *J. Struc. Engrg., ASCE*, Vol.124, No.5, 1997, pp.583~590.

4. Mirmiran, A., Shahawy, M., and Samaan, M., "Strength and ductility of hybrid FRP-concrete beam columns," *J. Struct. Engrg., ASCE*, Vol.125, No.10, 1999, pp.1085~1093.

5. Mirmiran, A., Shahawy, M., and Beitleman, T., "Slenderness limit for hybrid FRP-concrete columns," *J. Compos. for Constr., ASCE*, Vol.5, No.1, 2001, pp.26~34.

6. J. G. M. van Mier et al., "Strain-softening of concrete in uniaxial compression," *Materials and Structures*, RILEM, Vol. 30, No.198, May, 1997, pp.195~209.

7. Chen, W.F. and Lui, E.M. "Structural Stability," Elsevier, UK, 1987, pp.61~85.

8. *Development of durable glass fiber composite marine piles*, Research Report(IV), Structural safety research center at Kookmin university, Report for the Ministry of Maritime Affairs & Fisheries, 2002, pp.7~41.

9. Samaan, M., "*Analytical and experimental investigation of FRP concrete composite columns,*" Ph.D thesis, University of Central Florida, Orlando, Fla., 1997.

10. American Concrete Institute "*Building code requirements for structural concrete,*" ACI 318-02, American Concrete Institute, 2002, pp.126~133.